East European Journal of Physics. 1. 29–44 (2026)
DOI: 10.26565/2312-4334-2026-1-03 ISSN 2312-4334

OBSERVATIONAL CONSTRAINTS ON PLANE SYMMETRIC RENYI HOLOGRAPHIC DARK ENERGY UNIVERSE WITH SCALAR FIELDS AND COSMIC STRINGS

U.Y. Divya Prasanthi[1], **D. Tejeswararao**[2], **Mummidivarapu Nagaraju**[3], **Y. Aditya**[4,*], **G. Suryanarayana**[5]

[1]*Department of Statistics & Mathematics, College of Horticulture, Dr. Y.S.R. Horticultural University, Parvathipuram-535502, India*
[2]*Department of Basic Science and Humanities, GMR Institute of Technology (GMRIT) – Deemed to be University, Rajam-532127, India*
[3]*Department of Mathematics, Aditya University, Surampalem-533437, India*
[4]*Department of Mathematics, GMR Institute of Technology (GMRIT) – Deemed to be University, Rajam-532127, India*
[5]*Department of Mathematics, ANITS, Visakhapatnam-533003, India*
[*]*Corresponding Author e-mail: aditya.y@gmrit.edu.in; yaditya2@gmail.com*

Received September 24, 2025; revised January 29, 2026; accepted February 5, 2026

In this work, we investigate a cosmological model based on a plane symmetric space–time, where the matter content of the Universe is described by Rényi holographic dark energy within the framework of Einstein's theory of gravitation in the presence of massive scalar fields and cosmic strings. Exact solutions of the field equations are obtained by assuming a specific relation between the metric potentials. Observational constraints on the model parameters are obtained using the latest Hubble cosmic chronometer data through a Markov Chain Monte Carlo analysis. The resulting contour plots provide tight bounds on the free parameters, and the reconstructed Hubble parameter exhibits excellent agreement with the ΛCDM model over the entire redshift range. A detailed investigation of the cosmological parameters reveals that the model successfully reproduces the standard cosmic evolution. The deceleration parameter indicates a matter-dominated, decelerating phase at early epochs ($z \gtrsim 2$), followed by a smooth transition to the present accelerated phase and an asymptotic approach to a de Sitter–like expansion in the future. The dark energy equation of state parameter evolves dynamically and crosses the phantom divide, exhibiting quintom-like behavior. The ω_{de}–ω'_{de} plane analysis places the model predominantly in the freezing region, indicating a stable and rapidly accelerating dark energy phase. Statefinder diagnostics show consistency with ΛCDM at the present epoch, with deviations toward Chaplygin gas–like behavior at late times. Furthermore, the energy condition analysis supports the accelerated expansion through the violation of the strong energy condition at late times. Overall, the model provides a physically viable and observationally consistent description of cosmic evolution beyond the standard ΛCDM scenario.

Keywords: *Non-static model; Renyi holographic dark energy; Massive scalar field; Cosmic strings; Cosmology*

PACS: 98.80.-k, 95.36.+x

1. INTRODUCTION

The general theory of relativity (GR) has provided a robust framework to explain a wide range of cosmic phenomena, supported by substantial observational evidence. Astronomical observations [1, 2], most notably those of type-Ia supernovae (SNeIa) [3], indicate that the Universe is currently undergoing accelerated expansion. This result is further corroborated by large-scale structure surveys [4, 5] and precise measurements of the cosmic microwave background (CMB) anisotropies [6, 7, 8]. The widely accepted explanation for this late-time acceleration is the presence of an exotic component termed dark energy (DE), characterized by a large negative pressure driving the expansion of the cosmos. Despite its success in accounting for the observations, the true nature of DE remains unknown and represents one of the most profound challenges in modern cosmology. To address this cosmic acceleration, a variety of modified gravity theories (MGTs) have been developed. Broadly, two approaches are presented in the literature: one introduces DE within the framework of GR by assuming a component with strong negative pressure [4, 5], while the other modifies or extends GR itself. Recent studies indicate that such MGTs can successfully describe both the early Universe dynamics, such as inflation, and the present accelerated expansion, thereby offering a promising alternative to the ΛCDM paradigm.

From another perspective, the holographic DE (HDE) model [9] was proposed as a promising framework to explore the elusive nature of DE and to address certain theoretical challenges associated with the ΛCDM scenario. The central idea of the HDE model is rooted in the holographic principle, which asserts that the total energy contained within a region of size L should not exceed the mass of a black hole of the same size, i.e., $L^3\rho_{de} \leq LM_{pl}^2$. This inequality leads to the expression for the holographic DE density as

$$\rho_{de} = 3d^2M_{pl}^2L^{-2}, \tag{1}$$

where d^2 is a dimensionless constant, M_{pl} is the reduced Planck mass, and L represents the infrared (IR) cut-off scale.

Cite as: U.Y.Divya Prasanthi, D. Tejeswararao, Mummidivarapu Nagaraju, Y. Aditya, G. Suryanarayana, East Eur. J. Phys. 1, 29 (2026), https://doi.org/10.26565/2312-4334-2026-1-03

Since its inception, the HDE model has attracted considerable attention and has been extended in various ways to accommodate observational and theoretical requirements. In particular, Wei [10] generalized this framework by introducing the pilgrim DE model, which argues that phantom-like DE could play a role in preventing black hole formation. Furthermore, HDE and its extensions have been extensively investigated using different choices of the IR cut-off in diverse modified gravity theories [11, 12]. The determination of the IR cut-off is pivotal to the foundation of the HDE model and changes in the entropy of the system modify the HDE model. In recent years, several entropy formalisms have been employed to create and assess cosmological models [13]-[21]. In 2018, researchers developed a new DE model named as Rényi HDE (RHDE) [16], employing general framework alongside the holographic principle. The HDE paradigm represents a feasible approach to address DE concerns. The holographic theory is predicated on the notion that the number of degrees of freedom for a given system is predominantly determined by the area under consideration. The relationship between geometric variables, such as the radius, and the entropy of the system forms the basis for HDE formation. Tsallis ($\mathcal{S}_{\mathcal{T}}$) and Rényi ($\mathcal{S}_{\mathcal{R}}$) entropies serve as significant generalized entropy parameters, and their relationship is expressed as

$$\mathcal{S}_{\mathcal{R}}=\frac{1}{\delta}\, ln(1+\delta\mathcal{S}_{\mathcal{T}}) \tag{2}$$

$\mathcal{S}_{\mathcal{T}}=\frac{\mathcal{A}}{4}$. Here, $\mathcal{A}= 4\pi L^2$ and L represents the IR cutoff, constituting the Bekenstein entropy. We can ascertain the RHDE density utilizing the relation $\rho_{de}dV \propto T\, dS$ as:

$$\rho_{de}=\frac{3d^2}{L^2}(1+\pi\delta L^2)^{-1}. \tag{3}$$

Here, we adopt the RHDE model with the Hubble horizon cutoff $L = H^{-1}$. To ascertain the Hubble cutoff, we substitute it into Eq. (3) as

$$\rho_{de}=\frac{3d^2H^2}{1+\pi\delta H^{-2}}. \tag{4}$$

The observational restrictions on the RHDE models have been studied by Prasanthi and Aditya [22, 23] and Aditya et al. [24]. Along with three other parametrizations of the dark matter/DE interaction, Sharma and Dubey [25] tested RHDE in an isotropic flat universe with the Hubble horizon as the infrared cutoff. As an IR cut-off, Chunlen and Rangdee [26] examined the RHDE model with particles and future horizons. Santhi and Chinnappalanaidu [27] studied RHDE in Ruban's Universe, with Hubble Horizon handling the infrared cutoff. Rao et al. [28], Aditya [29] and Aditya et al. [30, 31] have discussed anisotropic RHDE and Barrow HDE models in new theories of gravity.

Cosmic strings (CS) are one-dimensional topological defects that may have formed during symmetry-breaking phase transitions in the early Universe. Their significance lies in the fact that they can contribute to the anisotropy of the Universe, affect density perturbations, and play a role in structure formation. Though current observations constrain their contribution to the energy density of the Universe, CS remain an important theoretical tool in connecting high-energy particle physics with cosmological dynamics. In particular, the interaction of CS with scalar fields can alter the expansion history and provide new insights into the role of topological defects in cosmology. The cosmological significance of topological defects has been comprehensively discussed by Vilenkin and Shellard [32] in their discussion. Their work provides a detailed theoretical framework describing the formation of topological defects during symmetry-breaking phase transitions in the early Universe, as well as their possible observational and cosmological implications. In particular, cosmic strings are shown to play a crucial role in connecting particle physics models with cosmological evolution and structure formation, motivating their inclusion in anisotropic and early-Universe cosmological scenarios. Letelier started the general relativistic study of strings (Letelier [33, 34]). The study of CS has since been pursued by a number of researchers in the presence of numerous physical sources and in a variety of alternative theories of gravitation, and literature containing relevant references is abound. CS in a five-dimensional spherically symmetric background under $f(R,T)$ gravity have been considered by Naidu et al. [35]. Accelerating Bianchi type (BT) DE models with CS in gravity have been examined by Shekh and Chirde [36]. BT-I string cosmological models in $f(R)$ gravity were studied by Aditya and Reddy [37]. Sahoo et al. [38] have investigated LRS BT – I model when the source of gravitation is a mixture of barotropic fluid and DE. Scalar fields (SFs) play a fundamental role in modern cosmology, providing a natural framework to explain various phases of cosmic evolution. A SF with mass, often referred to as a massive SF (MSF), is of particular importance due to its ability to influence both the early and late-time dynamics of the Universe. In the early Universe, MSFs are commonly associated with the mechanism of inflation. A slowly rolling MSF (the inflaton) can drive a rapid exponential expansion, solving key issues such as the horizon and flatness problems, while also generating the primordial density perturbations that seeded large-scale structure formation. The potential of a MSF, typically of the form $V(\phi) = \frac{1}{2}m^2\phi^2$, provides a simple yet effective description of inflationary dynamics. Furthermore, the coupling of MSFs with other cosmic ingredients, such as CS or anisotropic backgrounds, can introduce rich phenomenology. In anisotropic cosmologies, scalar fields can contribute to isotropization, while in the presence of topological defects like CS, they can influence the energy distribution and modify the expansion history.

The choice of a plane symmetric space-time offers a mathematically tractable framework to study anisotropic cosmologies. Unlike the isotropic FLRW metric, plane symmetry allows for directional dependence in the cosmic

expansion, thereby providing a more general background to investigate the effects of anisotropy. This is particularly important because observations of the cosmic microwave background (CMB) suggest small but non-negligible deviations from perfect isotropy. Plane symmetric models are therefore useful for probing the early anisotropic phases of the Universe and for analyzing how anisotropies decay over time to yield the present nearly isotropic Universe. The inclusion of massive scalar fields (MSFs), CS, and plane symmetric space-time in cosmological models provides a deeper understanding of the Universe's evolution by bridging high-energy physics with large-scale cosmology. Together, this framework offer a broader and more realistic picture of the Universe, capable of explaining both observational signatures and theoretical challenges beyond the standard ΛCDM model. Several researchers have investigated DE models with SFs in anisotropic backgrounds to gain deeper insights into cosmic evolution [39]-[49]. Naidu et al. [50] studied BT-V DE models in general relativity with scalar meson fields, while Reddy et al. [51] explored the Kantowski–Sachs DE model in the presence of scalar meson fields. Aditya et al. [52] analyzed the Kaluza–Klein DE model in the Lyra manifold with a large scalar field, and in the framework of $f(R,T)$ gravity, Aditya and Reddy [53] investigated the BT-III DE model in the presence of a MSF. Daniel Raju et al. [54]-[56] also considered various aspects of anisotropic DE models with MSFs. Furthermore, Aditya et al. [57] discussed the BT-VI_0 DE model with scalar fields, whereas Naidu et al. [58, 59] and Bhaskara Rao et al. [60, 61] investigated anisotropic minimally interacting DE models incorporating CS and MSFs. More recently, Aditya et al. [62, 63] studied anisotropic DE models with MSFs in Lyra geometry and in the context of $f(R,T)$ gravity. Motivated by the above discussion, the present work focuses on a non-static plane symmetric cosmological model of the Universe with CS, RHDE, and a MSF as sources of gravitation within the framework of Einstein's theory. The structure of the paper is organized as follows: Section-2 is devoted to the derivation and solution of the field equations. In section-3, we analyze the cosmological parameters of the model and discuss their physical significance. Finally, section-4 summarizes the conclusions of the study.

2. FIELD EQUATIONS AND MODEL

The structure of a non-static plane symmetric space-time is described by the following metric:

$$ds^2 = e^{2A}\{dt^2 - dr^2 - r^2d\theta^2 - B^2dz^2\}, \tag{5}$$

where A and B are the metric potentials depending solely on the cosmic time t.

Using this metric, Rao et al. [64] and Aditya et al. [65, 66] have investigated various cosmological models within the framework of different modified theories of gravity. In the presence of CS, a DE fluid, and an attractive massive scalar field, Einstein's field equations take the form (with the convention $8\pi G = c = 1$)

$$R_{ij} - \frac{1}{2}Rg_{ij} = -T_{ij}^{(tot)} \tag{6}$$

and energy conservation equation is given by

$$(T_{ij}^{(tot)})_{;j} = 0 \tag{7}$$

where $T_{ij}^{(tot)} = T_{ij}^{S} + T_{ij}^{de} + T_{ij}^{msf}$ is the total energy-momentum tensor of matter distribution of the universe. Here, and T_{ij}^{S}, T_{ij}^{de} and T_{ij}^{msf} are the energy-momentum tensors of strings, DE fluid and massive scalar fields respectively. These energy-momentum tensors are defined as follows:

$$\begin{aligned} T_{ij}^{S} &= \rho u_i u_j - \lambda x_i x_j, \quad u_i u^i = 1,\ x^i x_j = -1,\ u^i x_j = 0 \\ T_{ij}^{de} &= (\rho_{de} + p_{de})u_i u_j - g_{ij}p_{de} \\ T_{ij}^{msf} &= \phi_{,i}\phi_{,j} - \frac{1}{2}(\phi_{,k}\phi^{'k} - M^2\phi^2) \end{aligned} \tag{8}$$

here, p_{de} and ρ_{de} denote the pressure and energy density of the DE fluid, ϕ represents the MSF, λ corresponds to the string tension, and M is the mass of the scalar field. The Klein–Gordon equation governing the scalar field is given by

$$g^{ij}\phi_{;ij} + M^2\phi = 0. \tag{9}$$

The Einstein field equations (6), corresponding to the metric (5) and employing the relations (8)–(9), can be expressed as

$$\frac{1}{e^{2A}}\left[\dot{A}^2 + 2\frac{\dot{A}\dot{B}}{B} + 2\ddot{A} + \frac{\ddot{B}}{B}\right] + \frac{\dot{\phi}^2}{2} - \frac{M^2\phi^2}{2} = -\omega_{de}\rho_{de} \tag{10}$$

$$\frac{1}{e^{2A}}\left[\dot{A}^2 + 2\ddot{A}\right] + \frac{\dot{\phi}^2}{2} - \frac{M^2\phi^2}{2} = \lambda - \omega_{de}\rho_{de} \tag{11}$$

$$\frac{1}{e^{2A}}\left[3\dot{A}^2 + 2\frac{\dot{A}\dot{B}}{B}\right] - \frac{\dot{\phi}^2}{2} - \frac{M^2\phi^2}{2} = \rho + \rho_{de} \tag{12}$$

$$\ddot{\phi} + M^2\phi + \dot{\phi}\left(\frac{\dot{B}}{B} + 4\dot{A}\right) = 0. \tag{13}$$

The system of field equations (10)–(13) consists of four independent equations with seven unknown parameters, namely A, B, ϕ, ω_{de}, ρ_{de}, ρ, and λ. To obtain a complete solution of this system, three additional physically motivated conditions relating these parameters are required. In this work, we consider the following physically viable conditions:

(i) The shear scalar σ^2 is assumed to be proportional to the expansion scalar θ, which leads to the following relation between the metric potentials:

$$e^A = B^n, \tag{14}$$

where n is an arbitrary constant that preserves the anisotropic nature of the space-time. Since the present Hubble expansion of the universe is isotropic to within 30%, velocity–redshift observations for extragalactic sources are consistent with this assumption (Thorne [67]; Kantowski and Sachs [68]; Kristian and Sachs [69]). Moreover, redshift analyses indicate that for the present galaxy, the constraint $\frac{\sigma}{H} \leq 0.3$ holds. Collins, et al. [70] also showed that the normal congruence to homogeneous expansion satisfies the condition that $\frac{\sigma}{H}$ remains constant.

(ii) The average scale factor $a(t)$ and the scalar field ϕ are assumed to obey a power-law relation (Johri and Sudharsan [71]; Johri and Desikan [72]):

$$\phi \propto [a(t)]^k, \tag{15}$$

where k is the power-law index. Several authors have investigated different aspects of this relation in the literature [50]–[61]. Motivated by the physical relevance of Eq. (15), we adopt the following specific form to simplify the mathematical structure of the system:

$$\phi = \phi_0\,[a(t)]^k, \tag{16}$$

where ϕ_0 is a constant. Clearly, Eq. (16) is a direct consequence of the relation in Eq. (15).

Substituting Eqs. (14) and (16) into Eq. (13), the metric potentials can be obtained as

$$e^A = (\beta_1 \sinh(\beta_2 t + b_2))^{n\beta_3}, \quad B = (\beta_1 \sinh(\beta_2 t + b_2))^{\beta_3} \tag{17}$$

and scalar field ϕ can be obtained as

$$\phi = \phi_0\,(\beta_1 \sinh(\beta_2 t + b_2))^{\frac{k\beta_3(4n+1)}{3}} \tag{18}$$

where $\beta_1 = \left[\frac{-b_1 k(4n+1)^2(k+3)}{9M^2}\right]^{\frac{1}{2}}$, $\beta_2 = \left[\frac{-M^2(k+3)}{k}\right]^{\frac{1}{2}}$, $\beta_3 = \frac{3}{(4n+1)(k+3)}$, b_1 and b_2 are integrating constants. Since Pradhan et al. [73] and Mishra et al. [74] introduced an average scale factor of the form $a(t) = [\sinh(\alpha t)]^{\frac{1}{n}}$, in the study of DE models within anisotropic backgrounds, it is worth noting that the solution obtained here is both interesting and physically viable. Their analysis demonstrated that this choice of scale factor yields several possible scenarios consistent with present cosmological observations. In particular, the hyperbolic form of the scale factor has the advantage of naturally describing a transition from an early decelerated phase of cosmic evolution to the presently observed accelerated expansion, a feature strongly supported by supernovae Ia, CMB, and BAO data. In the literature, several authors have employed this hyperbolic scale factor to explore different facets of DE models [75]–[77], including the dynamics of anisotropic universes, the role of scalar fields, and modifications of general relativity. Consequently, investigating the scalar field model with the hyperbolic solution for the scale factor given in Eq. (17) provides not only mathematical tractability but also a physically compelling framework that aligns with current cosmological observations.

Now using Eq. (17) in Eq. (5) we can write our DE model as

$$ds^2 = (\beta_1 \sinh(\beta_2 t + b_2))^{2n\beta_3}\left\{dt^2 - dr^2 - r^2 d\theta^2 - (\beta_1 \sinh(\beta_2 t + b_2))^{2\beta_3} dz^2\right\}. \tag{19}$$

The metric (19) corresponds to a RHDE model involving the MSF (18) together with CS. In this context, the following dynamical parameters play a crucial role in the physical interpretation of the model. The Hubble parameter $H(z)$ can be obtained as

$$H = \left(\frac{4n+1}{3}\right)\beta_2\beta_3 \coth(\beta_2 t + b_2) = \left(\frac{4n+1}{3}\right)\beta_2\beta_3\left(1 + \frac{\beta_1^2}{(1+z)^{\frac{3}{\beta_3(4n+1)}}}\right)$$

$$= \frac{H_0}{(1+\beta_1^2)}\left(1+\frac{\beta_1^2}{(1+z)^{\frac{3}{\beta_3(4n+1)}}}\right)^{\frac{1}{2}}$$
$$= \frac{9H_0M^2}{9M^2-b_1k(4n+1)^2(k+3)}\left[1-\frac{b_1k(4n+1)^2(k+3)}{9M^2(1+z)^{k+3}}\right]. \quad (20)$$

where $1+z=\frac{1}{a}$ and H_0 is the present value (i.e., at $z=0$) of the Hubble parameter.

3. OBSERVATIONAL CONSTRAINTS

The field equations in self-creation theory of gravity have been solved exactly, and the resulting Hubble parameter contains the five model parameters (H_0, M, b_1, k, and n). Our aim is to constrain these parameters using observational Hubble datasets in order to validate the solution in the context of the present universe. In particular, we employ a joint analysis of 31 Hubble parameter data points from cosmic chronometer (CC) measurements [78, 79]. For the statistical analysis, we implement the `emcee` Python package, which performs Markov Chain Monte Carlo (MCMC) sampling. We explore the parameter space around the local minima by adopting a Gaussian prior centered on the initial estimates, with a fixed standard deviation of $\sigma=1.0$. The final results are presented through two-dimensional contour plots, showing the constraints on the model parameters with 1σ and 2σ confidence intervals. The chi-square function employed in the analysis is defined as

$$\chi^2_H(H_0,M,b_1,k,n)=\sum_{i=1}^{31}\frac{[H_{\rm th}(z_i;H_0,M,b_1,k,n)-H_{\rm obs}(z_i)]^2}{\sigma^2_{H(z_i)}}. \quad (21)$$

At each redshift z_i, the observed Hubble parameter is denoted by $H_{\rm obs}(z_i)$, while the theoretically predicted Hubble parameter, based on the model, is expressed as $H_{\rm th}(z_i;H_0,M,b_1,k,n)$. The corresponding observational uncertainty is represented by $\sigma_{H(z_i)}$. Using the CC datasets described above, we determine the best-fit values of the parameters H_0, M, b_1, k, and n. Figure 1 presents the results in the form of two-dimensional contour plots, displaying the parameter constraints with 1σ and 2σ confidence levels. The best-fit values are obtained as

Table 1. The MCMC estimates.

Datasets	Parameters	Prior	Value
Hubble (CC Data)	H_0	$(50,100)$	68.8 ± 1.5
	M	$(0,10)$	$+4.4\pm2.0$
	b_1	$(-5,3)$	$-2.4^{+1.3}_{-1.2}$
	k	$(-3,-2)$	$-2.22^{+0.27}_{-0.30}$
	n	$(0,2)$	$+1.07^{+0.29}_{-0.19}$

The contour plots in Fig. 1 illustrate the observational constraints on the model parameters. The following observations can be made from the contours. The allowed parameter space is tightly constrained around the best-fit values, demonstrating that the CC data provides significant restrictions on the model. This confirms the robustness of the dataset in probing late-time cosmic expansion. The best-fit values of the parameters lie well within the 1σ region, indicating that the model provides an excellent fit to the observational data. This strengthens the physical viability of the model when tested against Hubble expansion measurements. The fitting results are shown in Fig. 2, where the observational data points are compared with the theoretical predictions of our model as well as with the standard ΛCDM scenario. It is evident from the figure that the trajectory of our model lies very close to that of the ΛCDM model throughout the considered redshift range ($0<z<2$). This demonstrates that the model is consistent with the observed expansion history of the Universe. The agreement between our model and ΛCDM at low redshifts ($z<1$) is particularly strong, highlighting the model's ability to reproduce the late-time accelerated expansion, which is the main success of the cosmological constant scenario. At higher redshifts ($z>1$), slight deviations from ΛCDM can be observed. Such departures may provide additional degrees of freedom in describing the transition from the matter-dominated era to the present accelerating phase, without contradicting the available data.

4. COSMOLOGICAL PARAMETERS

We will discuss the physical meaning of dynamical parameters in our DE model in the presence of MSFs and CS in this section. To plot the behavior of cosmological parameters we use the values of model parameters as $H_0=68.8$,

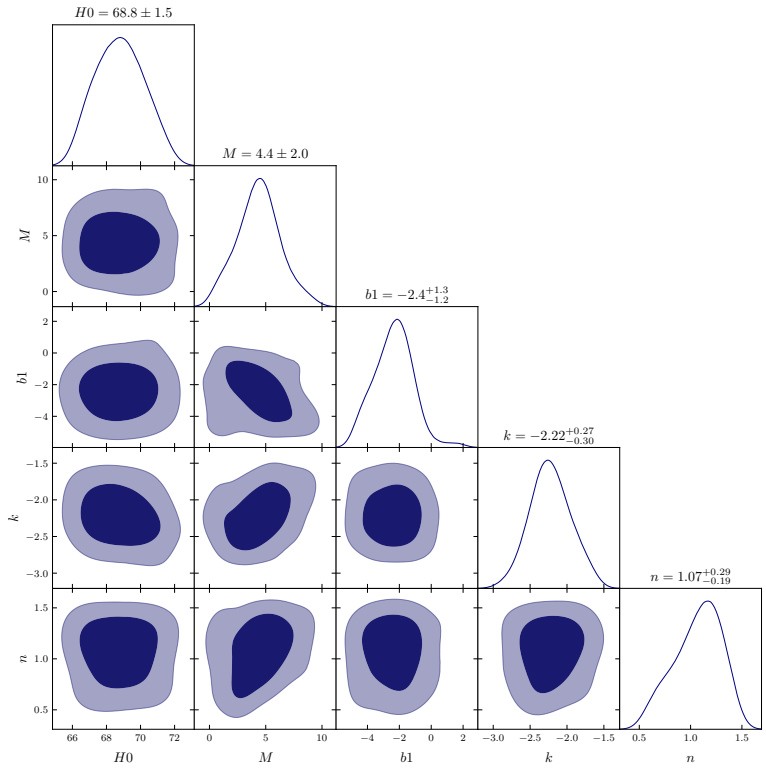

Figure 1. The plot displays the 2D contour plots of the model parameters.

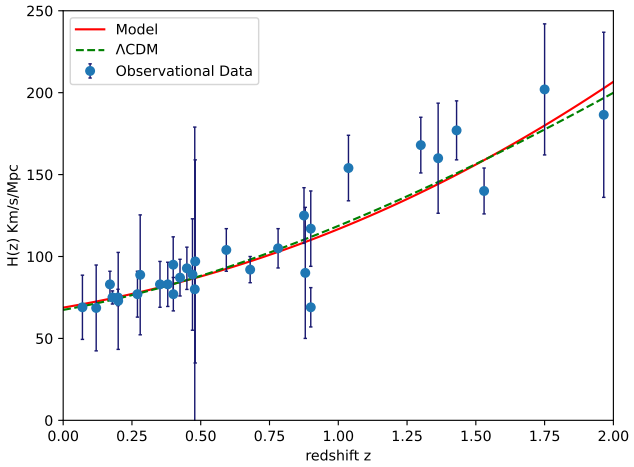

Figure 2. Evolution of Hubble parameter $H(z)$ versus redshift z. The solid line represents our model and dotted-line indicates the ΛCDM model with $\Omega_{m0} = 0.3$ and $\Omega_{\Lambda 0} = 0.7$. The dots are shown the Hubble dataset with error bar.

$M = 4.4$, $b_1 = -2.4$, $k = -2.22$, $n = 1.07$, $b_2 = 0.25$, $\phi_0 = 1 \times 10^{-7}$ and $\delta = 0.16$. The model's average scale factor ($a(t)$ and volume (V) are calculated as

$$V(t) = [a(t)]^3 = e^{4A}B = (\beta_1 \sinh(\beta_2 t + b_2))^{\frac{\beta_3(4n+1)}{3}} . \tag{22}$$

The expansion scalar θ are given by

$$\theta = \left(\frac{4n+1}{9}\right)\beta_2\beta_3 \coth(\beta_2 t + b_2) . \tag{23}$$

From Eqs. (4) and (23), we get the energy density of Renyi HDE of our model can be obtained as

$$\rho_{de} = 3\left(\frac{4n+1}{3}\right)^2 \beta_2^2\beta_3^2 \coth^2(\beta_2 t + b_2)\, d^2 \left(1 + \frac{9\pi\,\delta}{(4n+1)^2\,\beta_2{}^2\beta_3{}^2\,(\coth(\beta_2 t + b_2))^2}\right)^{-1} . \tag{24}$$

From Eqs. (11), (17) and (18) we obtain the string tension as

$$\lambda = \frac{-2n\beta_2^2\beta_3\, csch^2(\beta_2 t + b_2) + n^2\beta_2^2\beta_3^2\, \coth^2(\beta_2 t + b_2)}{(\beta_1 \sinh(\beta_2 t + b_2))^{2n\beta_3}} - \frac{-2n\beta_2^2\beta_3\, csch^2(\beta_2 t + b_2) + n^2\beta_2^2\beta_3^2\, \coth^2(\beta_2 t + b_2) + 2n\beta_2^2\beta_3^2\, \coth^2(\beta_2 t + b_2)}{(\beta_1 \sinh(\beta_2 t + b_2))^{2n\beta_3}} - \frac{\beta_2^2\beta_3\, csch^2(\beta_2 t + b_2) - \beta_2^2\beta_3^2\, \coth^2(\beta_2 t + b_2)}{(\beta_1 \sinh(\beta_2 t + b_2))^{2n\beta_3}}. \tag{25}$$

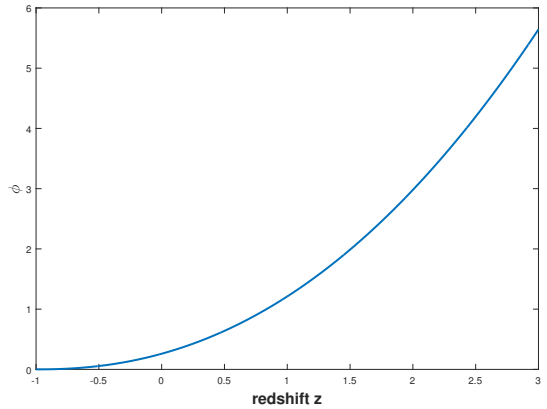

Figure 3. Plot of scalar field versus redshift.

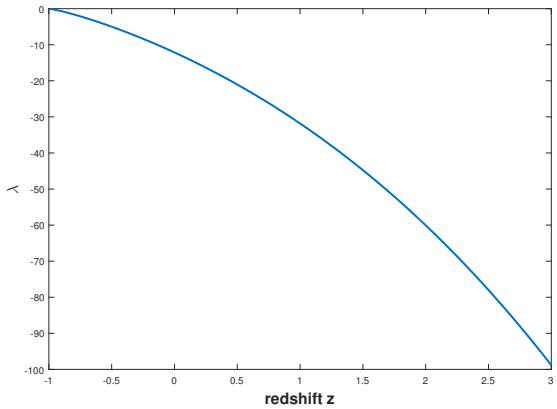

Figure 4. Plot of string tension density versus redshift.

Scalar field: The scalar field ϕ plays a fundamental role in cosmology, as it is capable of driving both the early inflationary phase and the late-time accelerated expansion of the Universe. Scalar fields play a significant role in modern cosmology, both theoretically and observationally. From a theoretical perspective, massive scalar fields naturally arise in scalar–tensor theories, modified gravity models, and higher-dimensional frameworks, where they act as additional gravitational degrees of freedom [80, 81]. In the early Universe, such fields can influence anisotropic dynamics and contribute to inflationary or pre-inflationary phases. At late times, massive scalar fields provide viable candidates for dynamical dark energy, allowing a time-dependent equation of state and enabling transitions between quintessence and phantom regimes [82, 83]. Observationally, the effects of massive scalar fields can be constrained through cosmic microwave background anisotropies, large-scale structure formation, and measurements of the expansion history using supernovae and Hubble cosmic chronometer data [84, 85]. Hence, massive scalar fields offer a physically well-motivated and observationally testable framework for describing the evolution of the Universe beyond the standard ΛCDM model. In the present model, the variation of ϕ with respect to the redshift z is depicted in Fig. 3. It is observed that the scalar field decreases monotonically with as universe evolves, starting from a high value at high redshift and attaining lowest values in the future ($z < 0$). Physically, this behaviour indicates that the scalar field was dominant in the early Universe, where its contribution to the energy density was more significant. As the Universe expanded toward the present epoch, the effective value of ϕ decreased, suggesting that its influence on the dynamics of cosmic evolution has gradually weakened. This is consistent with the idea that scalar fields could have played a key role in generating anisotropy and structure formation in the early epoch, while their contribution diminishes in the late-time Universe where DE becomes dominant.

String tension: The equation of state (EoS) of CS are restricted by the energy conditions. With $\rho > 0$ or $\lambda < 0$, the weak and strong energy conditions result in $\rho \geq \lambda$. The dominant energy conditions implies $\rho \geq 0$ and $\rho^2 \geq \lambda^2$. The signature of λ is not constrained by these energy conditions. The string tension density λ characterizes the tension or negative pressure along the direction of the strings and hence plays a significant role in determining the anisotropic nature of the Universe. In Fig. 4, the variation of λ with redshift z is displayed. It is observed that at high redshifts ($z \gtrsim 2$), the string tension density is strongly negative, with large magnitude. This suggests that in the early Universe, the contribution of string tension was significant, potentially dominating the anisotropic structure formation. As the Universe evolves towards lower redshifts, the magnitude of λ decreases monotonically. Around the present epoch ($z \approx 0$), the value of λ approaches zero, indicating that the influence of strings on the cosmic dynamics becomes negligible at late times. In the future epoch ($z < 0$), the string tension density continues to decay further toward zero, signifying that the Universe evolves toward an isotropic state where string effects vanish completely.

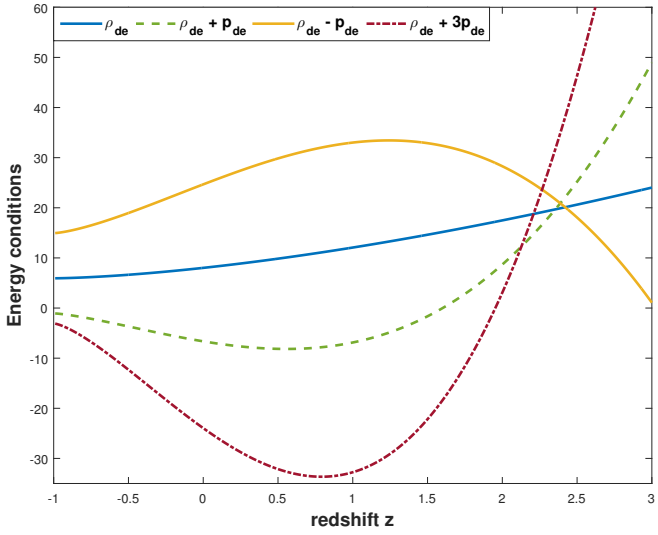

Figure 5. Plot of energy conditions versus redshift z.

Energy conditions: The energy conditions are powerful tools in general relativity and cosmology to examine the physical viability of matter and energy sources driving the cosmic dynamics. In the context of DE, these conditions provide insights into whether the model respects or violates classical energy requirements. The four commonly analyzed conditions are:

- Dominant Energy Condition (DEC): $\rho_{de} \geq 0,\ \rho_{de} \pm p_{de} \geq 0.$
- Strong Energy Condition (SEC): $\rho_{de} + p_{de} \geq 0,\ \rho_{de} + 3p_{de} \geq 0.$
- Null Energy Condition (NEC): $\rho_{de} + p_{de} \geq 0.$
- Weak Energy Condition (WEC): $\rho_{de} \geq 0,\ \rho_{de} + p_{de} \geq 0.$

In Fig. 5, the above conditions are tested for the model as a function of redshift z. In the framework of Self-Creation theory with RHDE, the evolution of energy conditions clearly reflects the cosmic history of the Universe. For $z > 0$, corresponding to the early epochs, the effective energy density ρ_{de} remains positive and the quantities $\rho_{de} + p_{de}$ and $\rho_{de} + 3p_{de}$ are also positive, ensuring the validity of the null, weak, and strong energy conditions. This behavior is consistent with a decelerated expansion dominated by matter and scalar field contributions. At the present epoch ($z = 0$), the energy density continues to be positive, while $\rho_{de} + 3p_{de}$ becomes negative, signaling the violation of the SEC. This violation marks the onset of late-time acceleration driven. For $z < 0$, representing the future evolution of the Universe, the continued violation of the NEC and SEC indicates a persistent phantom-like dark energy regime. Meanwhile, the DEC remains largely satisfied, ensuring causal energy flow. Overall, the energy conditions demonstrate a smooth transition from early-time deceleration to present and future accelerated expansion.

Deceleration parameter: The deceleration parameter $q(z)$ plays a crucial role in understanding the expansion dynamics of the Universe. By definition, it is expressed as

$$q(z) = -\frac{\ddot{a}a}{\dot{a}^2} = -1 + \frac{3\left(\text{sech}\left(\beta_2 t + b_2\right)\right)^2}{\beta_3\left(4n+1\right)} \tag{26}$$

where $a(t)$ is the scale factor, $\dot{a}$ is the expansion rate, and $\ddot{a}$ is the cosmic acceleration. The sign of $q(z)$ determines the nature of expansion. $q > 0$ corresponds to a decelerated Universe, $q = 0$ corresponds to a constant expansion rate, $-1 \leq q < 0$ indicates an accelerated expansion and $q < -1$ signifies a super-exponential or phantom-like expansion. From the plotted curve of $q(z)$ versus redshift z (see Fig. 6), the following physical interpretation can be made. At large redshift values (i.e., early epochs), the deceleration parameter is positive ($q > 0$), which corresponds to the decelerated phase. This behavior is consistent with a matter-dominated Universe, where the gravitational attraction of matter causes the expansion to slow down. Around $z \approx 1$, the curve crosses the line $q = 0$. This point indicates the transition redshift, marking the shift from decelerated expansion to accelerated expansion. Observational evidence from Type Ia supernovae and Cosmic Microwave Background measurements suggest that such a transition occurs within the range $0.5 \leq z_t \leq 1$. For smaller redshifts (at future epochs), the parameter falls into the range $-1 \leq q < 0$, which implies an accelerated expansion

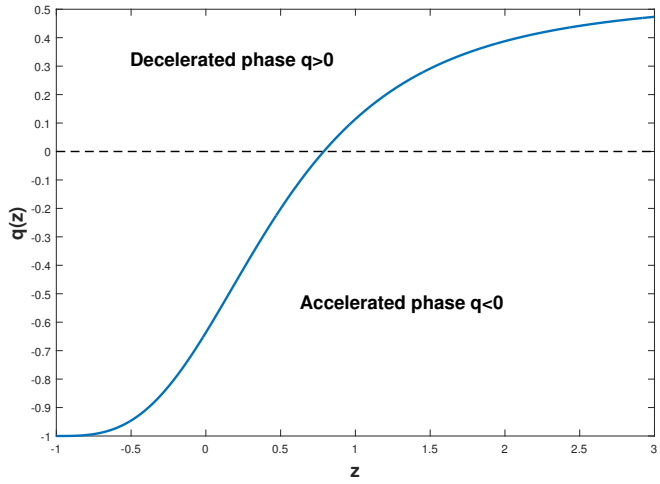

Figure 6. Plot of deceleration parameter versus redshift z.

phase. This is consistent with the presence of a DE component (such as a cosmological constant or a quintessence field) dominating the late-time cosmic dynamics. This suggests that the Universe will tend toward a de Sitter-like expansion, where the dynamics is dominated entirely by DE [86]-[89].

EoS parameter: The cosmic dynamics of the Universe can be effectively characterized by the equation of state (EoS) parameter $\omega = p/\rho$, where p and ρ represent the pressure and energy density of the cosmic fluid, respectively. Different values of ω correspond to distinct evolutionary phases of the Universe. For $\omega = 0$, the Universe is dominated by cold dark matter or dust-like fluid, giving rise to a decelerated expansion. When $0 < \omega \leq 1/3$, the dynamics correspond to the radiation-dominated era, with $\omega = 1/3$ exactly describing the radiation phase. For $\omega = 1$, the fluid is classified as stiff matter, which represents an extreme case of high-pressure matter content. For $\omega = -1$, the Universe corresponds to the cosmological constant (Λ) or vacuum energy, leading to exponential acceleration in a de Sitter phase. For $-1 < \omega < -1/3$, the expansion is accelerated and falls under the quintessence regime, where a dynamical scalar field drives the acceleration. For $\omega < -1$, the Universe enters the phantom regime, in which the energy density grows with time, potentially culminating in a "Big Rip" future singularity.

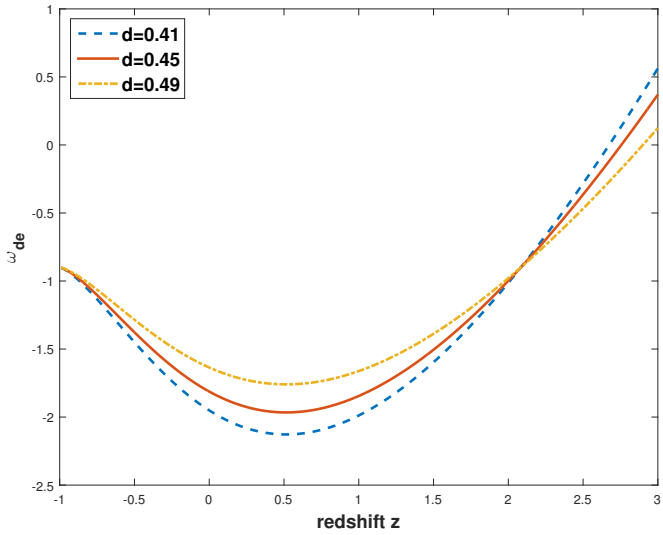

Figure 7. Plot of EoS parameter versus redshift z.

The EoS parameter (ω_{de}) of our model is obtained as

$$\omega_{de} = \frac{1}{3\left(\frac{4}{3}n+\frac{1}{3}\right)^2\beta_2^2\beta_3^2\coth^2(\beta_2 t+b_2)\,d^2}\Bigg[\frac{2n\beta_2^2\beta_3\,csch^2(\beta_2 t+b_2)-n^2\beta_2^2\beta_3^2\,\coth^2(\beta_2 t+b_2)}{\left(\beta_1\sinh(\beta_2 t+b_2)\right)^{2n\beta_3}}$$

$$-\frac{2n\beta_2^2\beta_3^2\,\coth^2(\beta_2 t+b_2)-\beta_2^2\beta_3\,csch^2(\beta_2 t+b_2)+\beta_2^2\beta_3^2\,\coth^2(\beta_2 t+b_2)}{\left(\beta_1\sinh(\beta_2 t+b_2)\right)^{2n\beta_3}}$$

$$+\tfrac{1}{2}M^2\phi_0^2\left(\beta_1\sinh(\beta_2 t+b_2)\right)^{\frac{2}{3}k\beta_3(4n+1)}$$

$$-\frac{\phi_0^2\left(\beta_1\sinh(\beta_2 t+b_2)\right)^{\frac{2}{3}k\beta_3(4n+1)}k^2\beta_3^2(4n+1)^2\beta_2^2\cosh^2(\beta_2 t+b_2)}{18\sinh^2(\beta_2 t+b_2)}\Bigg]$$

$$\times\left(1+\frac{\pi\delta}{\left(\frac{4}{3}n+\frac{1}{3}\right)^2\beta_2^2\beta_3^2\coth^2(\beta_2 t+b_2)}\right). \tag{27}$$

From Fig. 7, it is observed that at very high redshifts ($z \gtrsim 2$), the model effectively behaves close to the matter-dominated regime, ensuring consistency with the standard cosmological scenario. As the Universe evolves toward lower redshifts, the dark energy component becomes dynamically significant and the EoS parameter gradually shifts into the phantom region ($\omega_{de} < -1$), driving accelerated expansion. At the present epoch ($z = 0$), ω_{de} remains close to the cosmological constant boundary, in agreement with observational bounds. In the future evolution ($z < 0$), ω_{de} exhibits transitions between the quintessence ($-1 < \omega_{de} < -1/3$) and phantom regimes. This crossing of the phantom divide line characterizes a quintom-like behaviour, allowing a smooth transition between different acceleration phases while avoiding phantom domination.

Squared sound speed: An important diagnostic for testing the viability of DE models is the analysis of the squared sound speed $v_s^2 = \frac{\dot{p}_{de}}{\dot{\rho}_{de}} = \omega_{de} + \frac{\rho_{de}}{\dot{\rho}_{de}}\,\dot{\omega}_{de}$. The sign of v_s^2 plays a crucial role in determining the classical stability of perturbations. $v_s^2 > 0$ corresponds to a stable model where perturbations propagate without growing uncontrollably. $v_s^2 < 0$ indicates an unstable configuration, since perturbations tend to grow exponentially, leading to instabilities at the perturbative level.

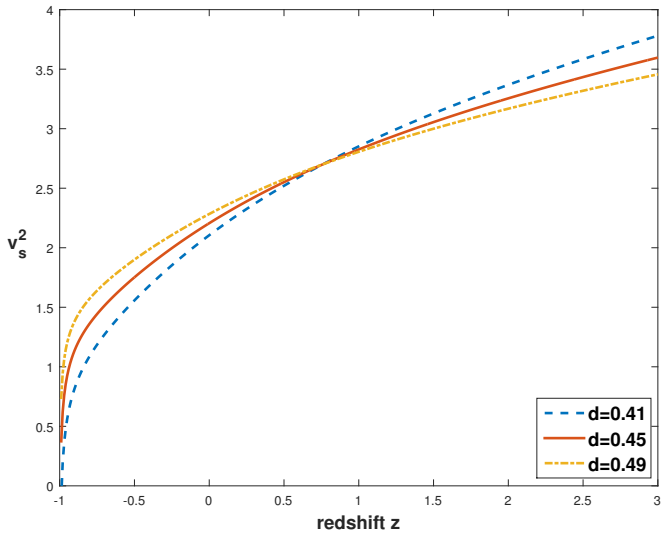

Figure 8. Plot of squared speed of sound versus redshift z.

In Fig. 8, the evolution of v_s^2 with redshift z is displayed for different values of the parameter d. It is evident that the squared speed of sound remains positive throughout the cosmic evolution for all considered parameter choices. In the early epochs ($z > 0$), particularly for $z \gtrsim 2$ corresponding to the matter-dominated era, v_s^2 maintains positive values, confirming that the model is dynamically stable during the decelerated expansion phase. At the present epoch ($z = 0$),

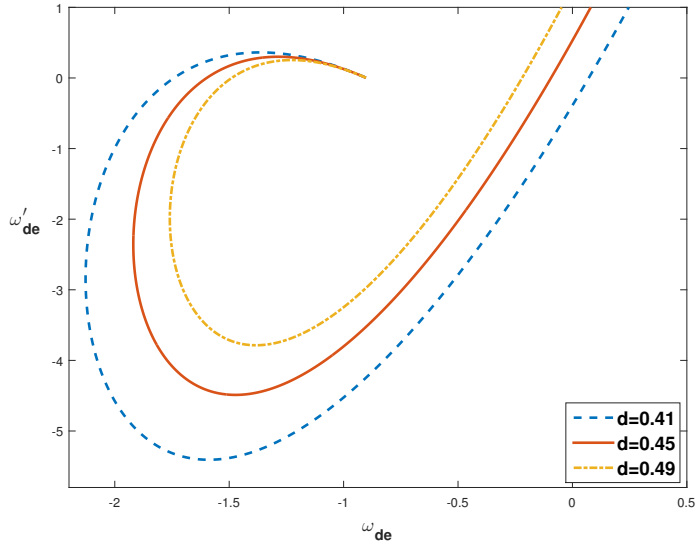

Figure 9. Plot of $\omega_{de} - \omega'_{de}$ plane.

v_s^2 continues to be positive, indicating that the current accelerated expansion driven by dark energy is free from classical instabilities. In the future evolution ($z < 0$), the squared sound speed remains positive and increases smoothly, suggesting that the dark energy fluid preserves its stability even in the late-time accelerated regime. Overall, the positivity of v_s^2 across all epochs demonstrates that the proposed model is classically stable and physically viable throughout the entire evolution of the Universe.

$\omega_{de} - \omega'_{de}$ **plane:** The dynamical nature of DE can be effectively studied through the $\omega_{de} - \omega'_{de}$ plane (Caldwell and Linder [90]), where ω_{de} is the equation of state (EoS) parameter and $\omega'_{de} = d\omega_{de}/d\ln a$ denotes its evolution with respect to the scale factor. This diagnostic is useful in distinguishing between different classes of DE models and their evolutionary behaviors. It is well established that the $\omega_{de} - \omega'_{de}$ plane can be divided into two distinct regions. Thawing region is characterized by ($\omega_{de} < 0,\ \omega'_{de} > 0$). In this regime, the DE equation of state parameter begins close to the cosmological constant value $\omega_{de} \simeq -1$ in the past and gradually increases towards higher values as the Universe evolves. Thawing models typically imply a slower rate of cosmic acceleration compared to freezing models, as the DE component evolves away from the cosmological constant behavior. Freezing region is characterized by ($\omega_{de} < 0,\ \omega'_{de} < 0$). In this regime, ω_{de} starts at values greater than -1 and gradually decreases towards -1 as the Universe evolves. Freezing models indicate a stronger acceleration rate, since the DE component asymptotically approaches a cosmological constant–like behavior in the far future.

From Fig. 9, it is observed that during the early epochs ($z > 0$), the trajectories of the model lie predominantly in the freezing region, characterized by $\omega_{de} < 0$ and $\omega'_{de} < 0$. This indicates that the dark energy component was dynamically evolving and contributed to a decelerated or mildly accelerated expansion while approaching a cosmological constant–like behavior. As the Universe evolves toward the present epoch ($z = 0$), the trajectories move closer to the boundary $\omega'_{de} = 0$, signifying a slowdown in the evolution of the equation of state parameter. In the future evolution ($z < 0$), the trajectories remain within the freezing region, implying that the dark energy gradually settles toward a stable attractor, typically associated with a de Sitter–like phase. This behavior corresponds to faster and sustained cosmic acceleration compared to thawing models. Hence, the $\omega_{de} - \omega'_{de}$ plane analysis confirms that the present model belongs to the freezing class of dark energy models, which is consistent with observational evidence of late-time accelerated expansion.

Statefinder parameters: The statefinder diagnostic, introduced by Sahni et al. [91] employs the pair of parameters (r, s) as a geometric tool to characterize and distinguish various DE models. These parameters are defined in terms of higher derivatives of the scale factor and provide a deeper insight into the cosmic expansion beyond the Hubble parameter and the deceleration parameter. They described as follows:

$$r = \frac{\dddot{a}}{aH^3}, \quad s = \frac{r-1}{3(q-\frac{1}{2})}. \tag{28}$$

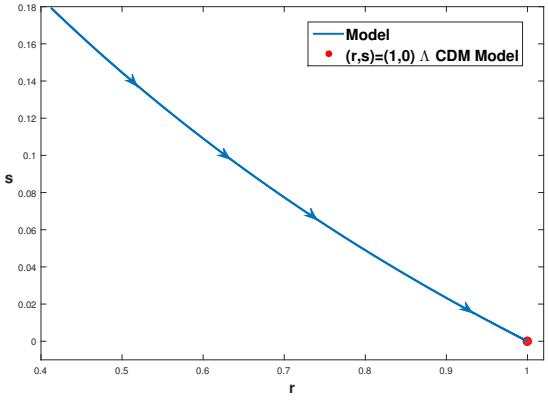

Figure 10. Plot of statefinder plane.

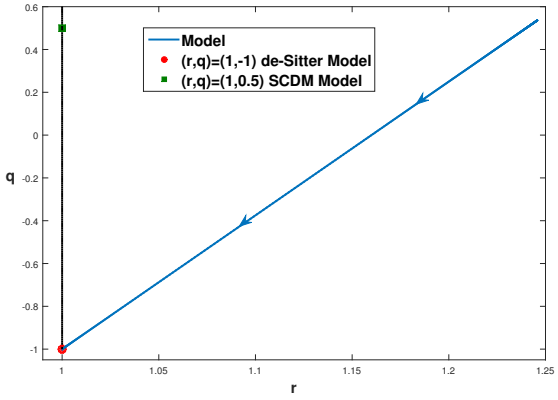

Figure 11. Plot of $r-q$ plane.

For our model statefinder parameters (r, s) are defined as

$$r = \frac{\left(\beta_1 \sinh(\beta_2 t + b_2)\right)^{\frac{1}{3}\beta_3(4n+1)}}{\left(\frac{4}{3}n + \frac{1}{3}\right)^3 \beta_2^3 \beta_3^3 \coth^3(\beta_2 t + b_2)} \left[\frac{1}{27} \frac{(4n+1)^3 \beta_2^3 \cosh^3(\beta_2 t + b_2)}{\beta_3^3 \sinh^3(\beta_2 t + b_2)}\right.$$
$$+ \frac{1}{3} \frac{(4n+1)^2 \beta_2^3 \cosh(\beta_2 t + b_2)}{\beta_3^2 \sinh(\beta_2 t + b_2)} - \frac{1}{3} \frac{(4n+1)^2 \beta_2^3 \cosh^3(\beta_2 t + b_2)}{\beta_3^2 \sinh^3(\beta_2 t + b_2)}$$
$$\left. - \frac{2}{3} \frac{\beta_3(4n+1)\beta_2^3 \cosh(\beta_2 t + b_2)}{\sinh(\beta_2 t + b_2)} + \frac{2}{3} \frac{\beta_3(4n+1)\beta_2^3 \cosh^3(\beta_2 t + b_2)}{\sinh^3(\beta_2 t + b_2)}\right]. \tag{29}$$

$$s = \left\{ \frac{\left(\beta_1 \sinh(\beta_2 t + b_2)\right)^{\frac{1}{3}\beta_3(4n+1)}}{\left(\frac{4}{3}n + \frac{1}{3}\right)^3 \beta_2^3 \beta_3^3 \coth^3(\beta_2 t + b_2)} \left[\frac{1}{27} \frac{(4n+1)^3 \beta_2^3 \cosh^3(\beta_2 t + b_2)}{\beta_3^3 \sinh^3(\beta_2 t + b_2)}\right.\right.$$
$$+ \frac{1}{3} \frac{(4n+1)^2 \beta_2^3 \cosh(\beta_2 t + b_2)}{\beta_3^2 \sinh(\beta_2 t + b_2)} - \frac{1}{3} \frac{(4n+1)^2 \beta_2^3 \cosh^3(\beta_2 t + b_2)}{\beta_3^2 \sinh^3(\beta_2 t + b_2)}$$
$$\left.\left. - \frac{2}{3} \frac{\beta_3(4n+1)\beta_2^3 \cosh(\beta_2 t + b_2)}{\sinh(\beta_2 t + b_2)} + \frac{2}{3} \frac{\beta_3(4n+1)\beta_2^3 \cosh^3(\beta_2 t + b_2)}{\sinh^3(\beta_2 t + b_2)}\right] - 1 \right\}$$
$$\times \left\{ 3 \left(-\frac{3}{2} + \frac{3\left(\operatorname{sech}(\beta_2 t + b_2)\right)^2}{\beta_3 (4n+1)} \right) \right\}. \tag{30}$$

Notably, for $(r, s) = (1, 0)$ the model corresponds to the ΛCDM model, $(r, s) = (1, 1)$ corresponds to the CDM model without a cosmological constant. If $s > 0$, the model resides in the phantom regime, while $r < 1$ places it in the quintessence region. Both these regions indicate DE dominance. If $s < 0$ and $r > 1$, the trajectory reflects Chaplygin gas behavior, which provides an effective unification of dark matter and DE. In the $r - s$ plane (see Fig. 10), the trajectory of the present model approaches to $(r, s) = (1, 0)$, indicating its close connection with the ΛCDM cosmology at late times. As the Universe evolves, the trajectory deviates from this fixed point and moves toward regions with $r > 1$ and $s < 0$, which are characteristic of Chaplygin gas-like behavior. This implies that the model accommodates a unifying picture of cosmic evolution, transitioning from a ΛCDM-like state to a regime reminiscent of generalized Chaplygin gas. The plotted trajectory shows that our model finally behaves like ΛCDM, then departs into the $(s < 0, r > 1)$ region, demonstrating Chaplygin gas–like characteristics. This transition highlights that the model does not remain locked into a pure ΛCDM phase but instead evolves dynamically, thereby offering a richer phenomenology that could address both the early decelerated phase and the late-time accelerated expansion.

$r - q$ plane: The $r - q$ plane provides a complementary diagnostic to probe the cosmic dynamics by combining the statefinder parameter r with the deceleration parameter q. This approach not only distinguishes between different

cosmological models but also highlights the dynamical evolution of the Universe across different epochs. In Fig. 11, two important fixed points are identified. $(r, q) = (1, 0.5)$ corresponds to the Standard Cold Dark Matter (SCDM) model without a cosmological constant. In this phase, the Universe is dominated by matter, and the positive value of q indicates a decelerating expansion. This fixed point characterizes the early-time behavior of the Universe where matter played the dominant role in governing the dynamics. $(r, q) = (1, -1)$ represents the de-Sitter model, which is a cosmological constant-dominated Universe. Here, $q = -1$ corresponds to an exponentially accelerating expansion, consistent with a late-time DE dominated phase.

The trajectory of the present model starts from the vicinity of the SCDM point $(r, q) = (1, 0.5)$, indicating that the early Universe underwent a decelerated matter-dominated phase. As cosmic time evolves, the trajectory moves downward along the $r - q$ plane and asymptotically approaches the de Sitter point $(r, q) = (1, -1)$. This evolution reflects a natural transition from the decelerating epoch of matter domination to the accelerating epoch driven by DE. Physically, this behavior is highly significant. The model not only replicates the expected decelerated expansion of the early Universe but also predicts the transition to an accelerated phase consistent with current observations of late-time cosmic acceleration. Moreover, the asymptotic approach to the de Sitter point suggests that the model tends toward a ΛCDM-like cosmology in the far future, where the expansion will be dominated by an effective cosmological constant.

5. RESULTS AND CONCLUSIONS

The accelerated expansion of the Universe has attracted considerable attention from researchers around the globe. Various approaches have been proposed to investigate this phenomenon, including modified theories of gravity and a wide range of dynamical DE models. In this work, we focus on a non-static plane symmetric cosmological model incorporating RHDE, an attractive MSF, and CS within the framework of Einstein's theory of gravity. Furthermore, we examine the behavior of well-known cosmological parameters and diagnostic planes in order to analyze the physical implications of the model. To assess the viability of the proposed DE model, we have analyzed a wide range of cosmological diagnostics, including background evolution, stability, and consistency with general relativity through energy conditions. The collective discussion emerging from these diagnostics can be summarized as follows:

- At higher redshifts, λ is strongly negative, indicating a significant role of CS in early anisotropic phases. Toward the present epoch and in the future, λ approaches zero, implying that string effects dilute over time, leading to an effectively isotropic Universe. The analysis of $\phi(z)$ suggests that the scalar field has a dual role. It may have contributed significantly to the early anisotropic expansion and structure formation, and later evolved into a subdominant but still relevant component in the present epoch. This behaviour supports the viability of MSFs as effective candidates for modeling both early and late-time cosmic acceleration.

- The model exhibits a transition from a decelerated phase ($q > 0$) at high redshifts, corresponding to matter domination, to an accelerated phase ($q < 0$) at low redshifts. The transition occurs around $z \sim 1$, in agreement with observational constraints from supernovae and CMB data. In the far future ($z < 0$), q asymptotically approaches -1, signaling a de Sitter-like accelerating state. The statefinder parameters (r, s) and (r, q) serve as higher-order diagnostics to distinguish our model from ΛCDM and other DE candidates. In the (r, s) plane, the trajectory approaches to $(1, 0)$ (the ΛCDM point) and moves into the $(s < 0, r > 1)$ region, characteristic of Chaplygin gas behavior. This indicates a dynamical evolution beyond the simple ΛCDM picture. In the (r, q) plane, the model interpolates between the SCDM fixed point $(1, 0.5)$, representing a decelerating matter-dominated phase, and the de-Sitter point $(1, -1)$, representing a DE-dominated accelerated phase. This confirms that the model captures the expected cosmic history.

- The analysis of the cosmological parameters demonstrates that the proposed model provides a consistent and physically viable description of the cosmic evolution. The equation of state parameter exhibits quintom-like behavior, allowing a smooth transition across the phantom divide and supporting late-time acceleration. The deceleration parameter confirms the transition from an early matter-dominated decelerated phase to the present accelerated epoch. Stability analysis based on the squared speed of sound shows that the model remains classically stable throughout the evolution. The energy condition analysis reveals a necessary violation of the strong energy condition at late times, while the weak and null energy conditions are largely satisfied, ensuring physical plausibility. Furthermore, the $\omega_{de} - \omega'_{de}$ plane places the model in the freezing region, indicating a stable approach toward a de Sitter–like accelerated phase. Overall, these results collectively confirm that the model successfully captures the essential features of cosmic acceleration and remains compatible with observational and theoretical expectations.

Finally, the model originates in a matter-dominated, decelerating phase, subsequently undergoes a quintom-like evolution, and asymptotically approaches a de Sitter–like state in the far future. The late-time violation of the strong and null energy conditions provides the necessary mechanism for accelerated expansion, while the progressive decay of string tension facilitates the isotropization of the Universe. Altogether, the proposed framework successfully reproduces the essential features of cosmic evolution and offers a rich phenomenology that extends beyond the standard ΛCDM paradigm.

Acknowledgments

Y. Aditya is thankful to the National Board for Higher Mathematics, Department of Atomic Energy, Govt. of India for its financial support under the grant No: 02011/8/2023 NBHM(R.P.)/R & D II/3073. The authors sincerely thank the anonymous reviewer for their constructive comments and valuable suggestions, which have significantly improved the quality and presentation of this work.

ORCID

U.Y. Divya Prasanthi, https://orcid.org/0009-0004-5397-050X; **D. Tejeswararao**, https://orcid.org/0000-0003-3508-346X; **Mummidivarapu Nagaraju**, https://orcid.org/0009-0008-7272-0169; **Y. Aditya**, https://orcid.org/0000-0002-5468-9697; **G. Suryanarayana**, https://orcid.org/0000-0002-4866-4020

REFERENCES

[1] M.S. Berman, Il Nuovo Cimento B, **74**, 182 (1983). https://doi.org/10.1007/bf02721676

[2] D. Saez, V.J. Ballester, Phys. Lett. A, **113**, 467 (1986). https://doi.org/10.1016/0375-9601(86)90121-0

[3] A.G. Riess, et al., Astron. J. **116**, 1009 (1998). https://doi.org/10.1086/300499

[4] M. Tegmark, et al., Phys. Rev. D, **69**, 103501 (2004). https://doi.org/10.1103/PhysRevD.69.103501

[5] U. Seljak, et al., Phys. Rev. D, **71**, 103515 (2005). https://doi.org/10.1103/PhysRevD.71.103515

[6] E. Komatsu, et al., Astrophys. J. Suppl. **180**, 330 (2009). https://doi.org/10.1088/0067-0049/180/2/330

[7] P. Ade, et al., Astron. Astrophys. **594**, A28 (2016). http://dx.doi.org/10.1051/0004-6361/201525819

[8] N. Aghanim, et al., Astron. Astrophys. **596**, A105 (2016). https://doi.org/10.1051/0004-6361/201628636

[9] M. Li, Phys. Lett. B, **603**, 1 (2004). https://doi.org/10.1016/j.physletb.2004.10.014

[10] H. Wei, Class. Quantum Grav. **29**, 175008 (2012). https://doi.org/10.1088/0264-9381/29/17/175008

[11] M. Sharif, and A.A. Jawad, Eur. Phys. J. C, **73**, 2382 (2013). https://doi.org/10.1140/epjc/s10052-013-2382-1

[12] M. Sharif, and S. Rani, J. Exp. Theor. Phys. **119**, 75 (2014). https://doi.org/10.1134/S1063776114070152

[13] M. Tavayef, et al., Phys. Lett. B, **781**, 195 (2018). https://doi.org/10.1016/j.physletb.2018.04.001

[14] C. Tsallis, and L.J.L. Cirto, Eur. Phys. J. C, **73**, 2487 (2013). https://doi.org/10.1140/epjc/s10052-013-2487-6

[15] A.S. Jahromi, et al., Phys. Lett. B, **780**, 21 (2018). https://doi.org/10.1016/j.physletb.2018.02.052

[16] H. Moradpour, et al., Eur. Phys. J. C, **78**, 829 (2018). https://doi.org/10.1140/epjc/s10052-018-6309-8

[17] S. Nojiri, et al., Phys. Rev. D, **105**, 044042 (2022). https://doi.org/10.1103/PhysRevD.105.044042

[18] S. Maity, and U. Debnath, Eur. Phys. J. Plus, **134**, 514 (2019). https://doi.org/10.1140/epjp/i2019-12884-6

[19] Y. Aditya, et al., East European Journal of Physics, **1**, 85 (2024). https://doi.org/10.26565/2312-4334-2024-1-06

[20] B.G. Rao, et al., East European Journal of Physics, **1**, 43 (2024). https://doi.org/10.26565/2312-4334-2024-1-03

[21] Y. Aditya, and U.Y.D. Prasanthi, Bulg. Astron. J. **38**, 52 (2023). https://astro.bas.bg/AIJ/issues/n38/YAditya.pdf

[22] U.Y. Divya Prasanthi, and Y. Aditya, Results Phys. **17**, 103101 (2021). https://doi.org/10.1016/j.rinp.2020.103101

[23] U.Y. Divya Prasanthi, and Y. Aditya, Phys. Dark Univ. **31**, 100782 (2021). https://doi.org/10.1016/j.dark.2021.100782

[24] Y. Aditya,, et al., Eur. Phys. J. C, **79(12)**, 1020 (2019). https://doi.org/10.1140/epjc/s10052-019-7534-5L

[25] U.K. Sharma, and V.Ch. Dubey, Int. J. Geom. Theor. Mod. Phys. **19(1)**, 2250010 (2022). https://doi.org/10.1142/S0219887822500104

[26] S. Chunlen, and P. Rangdee, Phayao Res. Conf. **10**, 2413 (2021). https://doi.org/10.48550/arXiv.2008.13730

[27] M.V. Santhi, and T. Chinnappalanaidu, *New Astron.* **92**, 101725 (2022). https://doi.org/10.1016/j.newast.2021.101725

[28] G.E. Rao, et al., Int. J. Math. Phys. **16**, 4 (2025). https://doi.org/10.26577/ijmph.20251611

[29] Y. Aditya, Bulg. Astron. J. **40**, 95 (2024). https://astro.bas.bg/AIJ/issues/n40/YAditya.pdf

[30] Y. Aditya, et al., AIP Conf. Proc. **3298**, 040005 (2025). https://doi.org/10.1063/5.0279440

[31] Y. Aditya, et al., Afrika Matematika, **36**, 120 (2025). https://doi.org/10.1007/s13370-025-01340-7

[32] A. Vilenkin, and E. P. S. Shellard, *Cosmic Strings and Other Topological Defects*, (Cambridge University Press, 2000).

[33] P.S. Letelier, Phys. Rev. D, **20**, 1294 (1979). https://doi.org/10.1103/PhysRevD.20.1294

[34] P.S. Letelier, Phys. Rev. D, **28**, 2414 (1983). ttps://doi.org/10.1103/PhysRevD.28.2414

[35] K.D. Naidu, et al., Astrophys. Space Sci. **363**, 158 (2018). https://doi.org/10.1007/s10509-018-3380-4

[36] S.H. Shekh, and V.R. Chirde, Astrophys. Space Sci. **365**, 60 (2020). https://doi.org/10.1007/s10509-020-03772-y

[37] Y. Aditya, and D.R.K. Reddy, Int. J. Geom. Theor. Mod. Phys. **15**, 1850156 (2020). https://doi.org/10.1142/S0219887818501566

[38] P. Sahoo, et al., Can. J. Phys. **98**, 109 (2020). https://doi.org/10.1139/cjp-2019-0494

[39] U.Y.D. Prasanthi, and Y. Aditya, Results Phys. **17**, 103101 (2020). https://doi.org/10.1016/j.rinp.2020.103101
[40] U.Y.D. Prasanthi, and Y. Aditya, Phys. Dark Univ. **31**, 100782 (2021). https://doi.org/10.1016/j.dark.2021.100782
[41] M.V. Santhi, et al., Can. J. Phys. **95**, 381 (2017). https://doi.org/10.1139/cjp-2016-0781
[42] M.V. Santhi, et al., Astrophys. Space Sci. **361**, 142 (2016). https://doi.org/10.1007/s10509-016-2731-2
[43] Y. Aditya, et al., Eur. Phys. J. C, **79**, 1020 (2019). https://doi.org/10.1140/epjc/s10052-019-7534-5
[44] Y. Aditya, and D.R.K. Reddy, Astrophys. Space Sci. **364**, 3 (2019). https://doi.org/10.1007/s10509-018-3491-y
[45] Y. Aditya, and D.R.K. Reddy, Eur. Phys. J. C, **78**, 619 (2018). https://doi.org/10.1140/epjc/s10052-018-6074-8
[46] K.D. Naidu, et al., Eur. Phys. J. Plus, **133**, 303 (2018). https://doi.org/10.1140/epjp/i2018-12139-2
[47] M.V. Santhi, et al., Int. J. Geom. Methods Mod. Phys. **15**, 1850161 (2018). https://doi.org/10.1142/S021988781850161X
[48] M.V. Santhi, et al., Int. J. Theor. Phys. **56**, 362 (2017). https://doi.org/10.1007/s10773-016-3175-8
[49] M.V. Santhi, et al., Can. J. Phys. **94**, 578 (2016). https://doi.org/10.1139/cjp-2016-0099
[50] R.L. Naidu, et al., Heliyon, **5**, e01645 (2019). https://doi.org/10.1016/j.heliyon.2019.e01645
[51] D.R.K. Reddy, et al., J. Dyn. Syst. Geom. Theor. **17**, 1 (2019). https://doi.org/10.1080/1726037X.2018.1551291
[52] Y. Aditya, et al., Astrophys. Space Sci. **364**, 190 (2019). https://doi.org/10.1007/s10509-019-3681-2
[53] Y. Aditya, and D.R.K. Reddy, Astrophys. Space Sci. **364**, 3 (2019). https://doi.org/10.1007/s10509-018-3491-y
[54] K. Deniel Raju, et al., Astrophys. Space Sci. **365**, 28 (2020). https://doi.org/10.1007/s10509-020-3729-3
[55] K. Deniel Raju, et al., Astrophys. Space Sci. **365**, 45 (2020). https://doi.org/10.1007/s10509-020-03753-1
[56] K. Deniel Raju, et al., Can. J. Phys. **98**, 993 (2020). https://doi.org/10.1139/cjp-2019-0563
[57] Y. Aditya, et al., Indian J. Phys. **95**, 383 (2021). https://doi.org/10.1007/s12648-020-01722-6
[58] K.D. Naidu, et al., Int. J. Mod. Phys. A, **36**(8), 2150054 (2021). https://doi.org/10.1142/S0217732321500541
[59] R.L. Naidu, et al., New Astron. **85**, 101564 (2021). https://doi.org/10.1016/j.newast.2020.101564
[60] M.P.V.V. Bhaskara Rao, et al., New Astron. **92**, 101733 (2022). https://doi.org/10.1016/j.newast.2021.101733
[61] M.P.V.V. Bhaskara Rao, et al., Int. J. Mod. Phys. A, **36**(36), 2150260 (2021). https://doi.org/10.1142/S0217751X21502602
[62] Y. Aditya, et al., Int. J. Mod. Phys. A, **37**(16), 2250107 (2022). https://doi.org/10.1142/S0217751X2250107X
[63] Y. Aditya, Bulg. Astron. J. **39**, 12 (2023). https://astro.bas.bg/AIJ/issues/n39/YAditya.pdf
[64] V.U.M. Rao, et al., Results Phys. **10**, 469 (2018). https://doi.org/10.1016/j.rinp.2018.06.027
[65] Y. Aditya, et al., Results Phys. **12**, 339 (2019). https://doi.org/10.1016/j.rinp.2018.11.074
[66] Y. Aditya, et al., New Astron. **84**, 101504 (2021). https://doi.org/10.1016/j.newast.2020.101504
[67] K.S. Thorne, Astrophys. J. **148**, 51 (1967). https://ui.adsabs.harvard.edu/link_gateway/1967ApJ...148...51T/doi:10.1086/149127
[68] R. Kantowski, and R.K. Sachs, J. Math. Phys. **7**, 433 (1966). https://doi.org/10.1063/1.1704952
[69] J. Kristian, and R.K. Sachs, Astrophys. J. **143**, 379 (1966). https://doi.org/10.1086/148522
[70] C.B. Collins, et al., Gen. Relativ. Gravit. **12**, 805 (1980). https://doi.org/10.1007/BF00763057
[71] V.B. Johri, and K. Desikan, Gen. Relativ. Gravit. **26**, 1217 (1994). https://doi.org/10.1007/BF02106714
[72] V.B. Johri, and R. Sudharsan, Aust. J. Phys. **42**, 215 (1989). https://doi.org/10.1071/PH890215
[73] A. Pradhan, et al., Astrophys. Space Sci. **337**, 401 (2012). https://doi.org/10.1007/s10509-011-0835-2
[74] R.K. Mishra, et al., Int. J. Theor. Phys. **52**, 2546 (2013). https://doi.org/10.1007/s10773-013-1540-4
[75] V.U.M. Rao, and U.Y. Divya Prasanthi, Eur. Phys. J. Plus, **132**, 64 (2017). https://doi.org/10.1140/epjp/i2017-11328-9
[76] H. Amirhashchi, et al., Int. J. Theor. Phys. **50**, 3529 (2011). https://doi.org/10.1007/s10773-011-0861-4
[77] R.K. Mishra, et al., Int. J. Theor. Phys. **55**, 1241 (2016). https://doi.org/10.1007/s10773-015-2766-0
[78] J. Simon, L. Verde, and R. Jimenez, Phys. Rev. D, **71**, 123001 (2005). https://doi.org/10.1103/PhysRevD.71.123001
[79] G.S. Sharov, and V.O. Vasiliev, Math. Model. Geom. **6**, 1 (2018). https://doi.org/10.26456/mmg/2018-611
[80] C. Brans, and R. H. Dicke, Phys. Rev. **124**, 925 (1961). https://doi.org/10.1103/PhysRev.124.925
[81] V. Faraoni, Cosmology in Scalar-Tensor Gravity, (Springer, 2004).
[82] R. R. Caldwell, et al., Phys. Rev. Lett. **80**, 1582 (1998). https://doi.org/10.1103/PhysRevLett.80.1582
[83] B. Feng, et al., Phys. Lett. B, **607**, 35 (2005). https://doi.org/10.1016/j.physletb.2004.12.071
[84] N. Aghanim, et al., Astron. Astrophys. **641**, A6 (2020). https://doi.org/10.1051/0004-6361/201833910
[85] M. Moresco, et al., JCAP, **05**, 014 (2016). https://doi.org/10.1088/1475-7516/2016/05/014
[86] J.V. Cunha, Phys. Rev. D, **79**, 047301 (2009). https://doi.org/10.1103/PhysRevD.79.047301
[87] Z. Li, et al., Phys. Lett. B, **695**, 1 (2011). https://doi.org/10.1016/j.physletb.2010.10.044

[88] H. Amirhashchi, and S. Amirhashchi, Phys. Rev. D, **99**, 023516 (2019). https://doi.org/10.1103/PhysRevD.99.023516

[89] S. Capozziello, et al., Mon. Not. R. Astron. Soc. **484**, 4484 (2019). https://doi.org/10.1093/mnras/stz176

[90] R.R. Caldwell, and E.V. Linder, Phys. Rev. Lett. **95**, 141301 (2005). https://doi.org/10.1103/PhysRevLett.95.141301

[91] V. Sahni, et al., J. Exp. Theor. Phys. Lett. **77**, 201 (2003). https://doi.org/10.1134/1.1574831

ОБМЕЖЕННЯ СПОСТЕРЕЖЕНЬ НА ПЛОСКОМУ СИМЕТРИЧНОМУ ГОЛОГРАФІЧНОМУ ВСЕСВІТІ ТЕМНОЇ ЕНЕРГІЇ РЕНЫ ЗІ СКАЛЯРНИМИ ПОЛЯМИ ТА КОСМІЧНИМИ СТРУНАМИ

У.Й. Дів'я Прасанті[1], **Д. Техесварарао**[2], **Муммідіварапу Нагараджу**[3], **Ю. Адітья**[4], **Г. Сурьянарараяна**[5]

[1]*Департамент статистики & математики, коледж садівництва, Dr. Y.S.R. Садівничий університет, Парватіпурам-535502, Індія*

[2]*Кафедра фундаментальних та гуманітарних наук, Технологічний інститут GMR (GMRIT) – вважається університетом, Раджам-532127, Індія*

[3]*Кафедра математики, Університет Адітья, Сурампалем-533437, Індія*

[4]*Кафедра математики, Технологічний інститут GMR (GMRIT) – вважається університетом, Раджам-532127, Індія*

[5]*Кафедра математики, ANITS, Вішакхапатнам-533003, Індія*

У цій роботі ми досліджуємо космологічну модель, засновану на плоскому симетричному просторі-часі, де вміст речовини у Всесвіті описується голографічною темною енергією Реньї в рамках теорії гравітації Ейнштейна за наявності масивних скалярних полів та космічних струн. Точні розв'язки рівнянь поля отримуються, припускаючи певне співвідношення між метричними потенціалами. Спостережувальні обмеження на параметри моделі отримані з використанням найновіших даних космічного хронометра Хаббла за допомогою аналізу Монте-Карло методом ланцюгів Маркова. Отримані контурні графіки забезпечують чіткі межі для вільних параметрів, а реконструйований параметр Хаббла демонструє чудову узгодженість з моделлю ΛCDM у всьому діапазоні червоного зміщення. Детальне дослідження космологічних параметрів показує, що модель успішно відтворює стандартну космічну еволюцію. Параметр уповільнення вказує на фазу уповільнення з домінуванням матерії на ранніх епохах ($z \gtrsim 2$), після чого відбувається плавний перехід до поточної прискореної фази та асимптотичний наближення до розширення, подібного до де Сіттера, у майбутньому. Параметр рівняння стану темної енергії динамічно еволюціонує та перетинає фантомний вододіл, демонструючи поведінку, подібну до квінтома. Аналіз площини ω_{de}–ω'_{de} розміщує модель переважно в області замерзання, що вказує на стабільну та швидко прискорюючу фазу темної енергії. Діагностика Statefinder показує узгодженість з ΛCDM у сучасну епоху, з відхиленнями в бік поведінки, подібної до газоподібної Чаплигіна, на пізніх етапах часу. Крім того, аналіз енергетичних умов підтримує прискорене розширення через порушення сильного енергетичного стану на пізніх етапах часу. Загалом, модель забезпечує фізично життєздатний та спостережливо узгоджений опис космічної еволюції поза стандартним сценарієм ΛCDM.

Ключові слова: *нестатична модель; голографічна темна енергія Реньї; масивне скалярне поле; космічні струни; космологія*